Predictions of Flow Behaviors and Entrance Pressure Drop Characteristics of a Rubber Compound in a Capillary Die Using Various Rheological Models

J.H. Kim,[1] **M.Y Lyu**[2]
[1] *LG Electronics, Gyeonggi-do, South Korea*

[2] *Department of Mechanical System Design Engineering, Seoul National University of Science and Technology, Seoul, South Korea*

Rubber compounds have highly viscoelastic properties. The viscoelastic behaviors that have been exhibited during die extrusion include die swell and vortices in regions of sudden contraction. In this study, the application of rheological models to the capillary die extrusion process is investigated. Experiments and simulations were conducted using a fluidity tester and finite element analysis, respectively. The velocity distributions, velocity profiles, pressure drops, and vortices at the capillary die entrance were analyzed through computer simulations for various viscoelastic models [i.e., Phan-Thien and Tanner (PTT), Giesekus, POMPOM, simplified viscoelastic, and generalized Newtonian models]. Different models exhibited different pressure drops and different velocity profiles in the capillary die. Only the full viscoelastic models (PTT, Giesekus, and POMPOM) predicted the vortex at the corner of the reservoir that is the capillary die entrance. However, the simplified viscoelastic and generalized Newtonian models did not predict the vortex. All the viscoelastic models studied in this article predicted the die swells in various ways, and these were compared with the experimental results. The PTT and simplified viscoelastic models exhibited good agreement with the experimental results of the die swells. **POLYM. ENG. SCI., 54:2441–2448, 2014.**

INTRODUCTION

Computer simulations are used widely in science and engineering to solve problems and understand physical behaviors. The accuracy of the simulation results depends on the numerical computations and theoretical models that describe the subjected problem. Rubbers, rubber compounds, and elastomers are highly viscoelastic materials that exhibit complex flow behaviors, such as die swell, vortices in regions of sudden contraction, and normal stress differences [1–3]. Because these factors are involved, die design for the extrusion of rubber compounds is very complicated. Thus, the role of computer simulations is increasingly important in this area. Predictions of velocity contours, pressure profiles, and pressure drops along the direction of flow are considered significant information for die design.

Correspondence to: Min-Young Lyu; e-mail: mylyu@seoultech.ac.kr
Contract grant sponsor: Ministry of Knowledge Economy (MKE) (World Class-300 Project in Knowledge Economy Technology Innovation Program and New Growth Power Equipment Competitiveness Reinforcement Program).
DOI 10.1002/pen.23785
Published online in Wiley Online Library (wileyonlinelibrary.com).

Early research on simulation of viscoelastic flow primarily focused on computing methods such as elastic-viscous stress-splitting and finite element formulations [1–3]. Hulsen investigated the elastic and elongational properties of rubber compounds in viscoelastic simulations using the Galerkin finite element method [4]. Lee and coworkers published articles in which way they simulated nonisothermal viscoelastic flows and proposed a time-Weissenberg number superposition [5, 6]. However, these studies were limited to a few viscoelastic models [i.e., Phan-Thien and Tanner (PTT), upper convected Maxwell, and Oldroyed-B] with one or two relaxation modes and simple geometries [7–11]. Furthermore, research that uses computer simulations for profile extrusion has been published [12–14]. Viscoelastic simulations involving parameter studies of viscoelastic models have also been published [15, 16]. Recently, intensive studies on capillary die extrusion have been published by Hatzikiriakos and Mitsoulis's group [17–22]. Their research included both experimental and theoretical treatment of die swell, vortices, and pressure drops at the die entrance. Viscoelastic simulations using the PTT model demonstrated the die swell and vortex at the die entrance for various flow rates, die lengths, and relaxation modes for a rubber compound [23–25].

There has been a significant amount of research on the die swell in capillary die extrusion using several different polymers [23–34]. Die swell is primarily a function of the shear rate and temperature among the operating parameters, but is also a function of the die length and reservoir size. Generally, die swell increases as the shear rate increases [2, 26, 27], and decreases as the temperature increases because its elastic properties are diminished as the temperature increases [2, 27, 28, 31, 35]. Furthermore, the die swell decreases as the die length or die length ratio to die diameter (*L*/*D*) increases because the material can be more relaxed in a longer die [2, 27]. This infers that the die swell decreases as the residence time in the die increases, which can also be interpreted as the material having a decaying memory. Furthermore, the larger the diameter of the reservoir, the bigger the die swell [2, 36, 37].

In profile extrusion, the above mentioned parameters affect the extrudate profile and the prediction of the extrudate profile is not simple; thus, computer simulations are important in predicting it. Numerical computer simulations for profile extrusion have been published [12–14, 38–41], and most of these published studies have focused on the numerical scheme and geometry of the die. The discussions of the computation results have primarily focused on the die

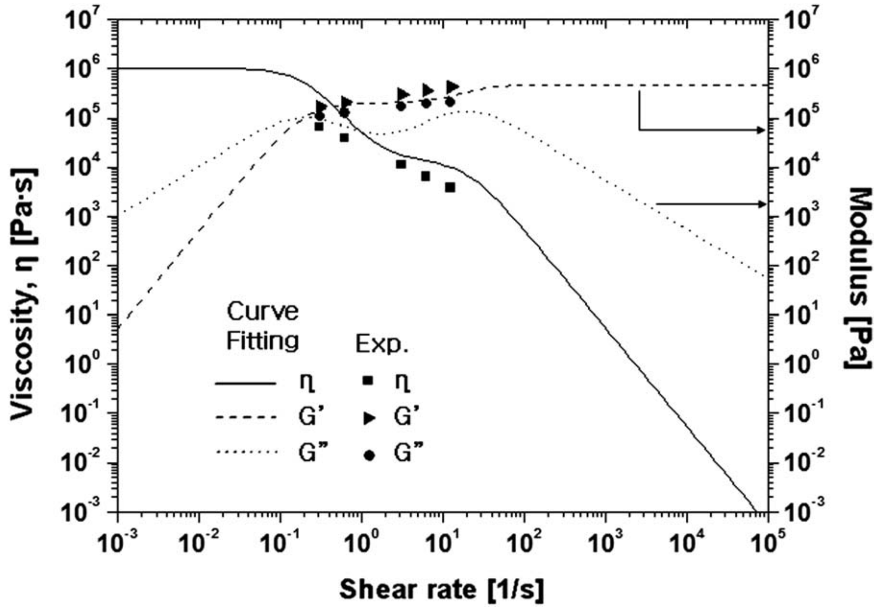

FIG. 1. Shear viscosity, storage and loss modulus of the rubber compound used in this study.

swell and the vortices near the die entrance. However, the velocity and pressure profiles along the flow direction and the pressure drop characteristics near the die entrance have not yet been discussed according to the rheological models.

Therefore, this research is an extension of previous work [23]. A computer simulation of flow in the capillary die was performed; various viscoelastic models including the PTT, Giesekus, POMPOM, and simplified viscoelastic models were used to simulate the flow behavior of a rubber compound in a capillary die using a full three-dimensional (3D) geometric model. The generalized Newtonian model was also used for comparison with the viscoelastic models. The velocity profiles, pressure distributions, pressure drops, and vortices at the capillary die entrance are discussed extensively for various rheological models.

EXPERIMENTAL AND SIMULATIONS

Materials and Capillary Extrusion

The rubber compound used in this experiment consisted of 90% styrene butadiene rubber (SBR) and 10% butadiene rubber (BR). The viscosity, storage, and loss moduli were measured using an oscillatory rheometer (Rubber Process Analyser, RPA 2000; Monsanto, USA). Figure 1 shows the viscosity, storage (G'), and loss moduli (G'') of the rubber compound at 110°C. These material properties were measured for frequency and the frequency was converted to the shear rate. Figure 1 also shows predicted properties for the PTT model. Details are explained in the next section.

For the capillary extrusion, a fluidity tester (Automatic Fluidmeter, Taegun Engineering Co., South Korea) was used. Figure 2 shows the computer modeling of the fluidity tester used for simulation. It consists of a reservoir and a capillary die and is equipped with a laser to measure the die swell. The rubber compound in the reservoir is pressed into the capillary die by the plunger. The diameter and length of the reservoir are both 25 mm; those of the capillary die are both 2.5 mm. The temperature of the reservoir and capillary die was set to 110°C during the extrusion experiment. The swollen diameters of the extruded rubber compound were measured according to the plunger speed using laser equipment.

Computer Simulation of Extrusion

Modeling for the Finite Element Analysis and Boundary Conditions. Figure 2 shows the mesh used in the finite element analysis (FEA) of the die extrusion. One-quarter of the total region was used for the full 3D viscoelastic isothermal

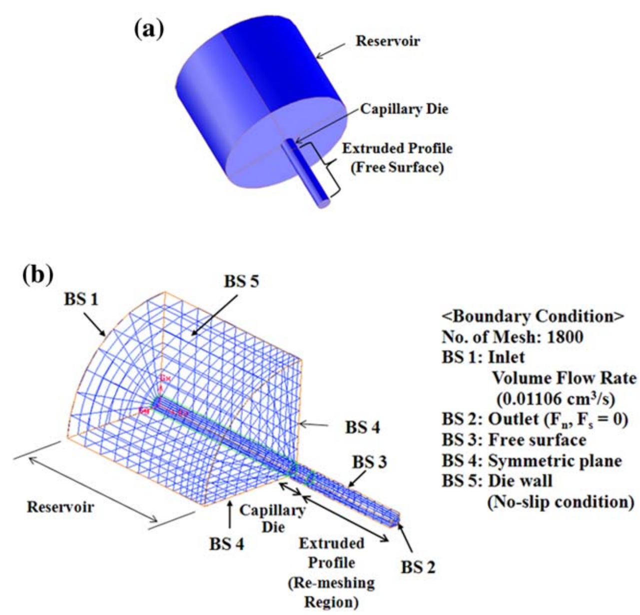

FIG. 2. Three-dimensional modeling, mesh, and boundary conditions for the simulations. (a) Computer modeling of the fluidity tester for the simulations. (b) Mesh and boundary conditions for the flow simulations. [Color figure can be viewed in the online issue, which is available at wileyonlinelibrary.com.]

 DOI 10.1002/pen

TABLE 1. Parameters for rheological models used in this study.

PTT	1-mode	2-mode	3-mode
ε	0.010353	0.010353	0.010353
λ	0.0062	0.01854993	0.0555
η	5.238462	2.462002	115769.8
ξ	0.20706	0.20706	0.31059
Giesekus	1-mode	2-mode	3-mode
η	3.982645	7.813225	106688.2
λ	0.004625	0.0185	0.074
α	0.20706	0.20706	0.31059
POMPOM	1-mode	2-mode	3-mode
λ	0.0062	0.0185	0.0555
G	819	126	204194
λa	0.0032	0.0104	0.0107
q	2.11	2.28	2.06
ξ	0.1074	0.1162	0.1161

Simplified Viscoelastic		Generalized Newtonian	
$\eta\infty$	0.00006664937	$\eta\infty$	0.00006664937
η_0	1625461.1	η_0	1625461.1
λ	100	λ	100
n	0.2238212	n	0.2238212
Ψ	0.62		

analysis using a commercial program (Polyflow, Fluent, Belgium). The flow rate was imposed on the inlet area denoted by BS 1 and the outflow condition was imposed on the exit area denoted by BS 2. The free boundary surface condition was set to the extrudate surface (BS 3). The symmetry condition was set to two symmetry surfaces (BS 4) and no-slip conditions were set to the die wall (BS 5). Remeshing was performed during the calculation of the free surface of the extrudate (BS 3) using the "optimesh" function provided in Polyflow.

Rheological Model. Nonlinear viscoelastic models (i.e., PTT, Giesekus, POMPOM, and simplified viscoelastic) were used to simulate the viscoelastic flow behavior of the rubber compound in the capillary die.

Equation 1 represents the PTT model [40–42]:

$$T = T_1 + T_2 \tag{1a}$$

$$T_2 = 2\eta_2 D \tag{1b}$$

$$\eta_2 = r_\eta \eta \tag{1c}$$

$$r_\eta = \eta_2/\eta \tag{1d}$$

$$T_1 = \exp\left[\frac{\varepsilon\lambda}{\eta_1} tr(T_1)\right] + \lambda\left[\left(1-\frac{\xi}{2}\right)\overset{\nabla}{T_1} + \frac{\xi}{2}\overset{\nabla}{T_1}\right] = 2\eta_1 D \tag{1e}$$

The extra stress (T) is the sum of T_1 and T_2. T_1 is a viscoelastic component and T_2 is a purely viscous component. η_2 is a viscosity factor for the Newtonian (i.e., purely viscous) component of the extra-stress tensor. The viscosity ratio (r_η) is defined in *Eq. 1d*. The extensional flow of the material is set by control parameter ε, λ is relaxation time, ξ is a shear viscosity control parameter, and D is the deformation rate. Parameters used in this study for PTT model are summarized in Table 1.

The Giesekus model can be expressed as [1, 43]:

$$T = T_1 + T_2 \tag{2a}$$

$$T_2 = 2\eta_2 D \tag{2b}$$

$$\left(\mathrm{I} + \frac{\alpha\lambda}{\eta_1}\mathrm{T}_1\right)\cdot \mathrm{T}_1 + \lambda\overset{\nabla}{T_1} = 2\eta_2 D \tag{2c}$$

where α is a material constant that controls the extension viscosity.

The POMPOM model is expressed as [43, 44]:

$$T = T_1 + T_2 \tag{3a}$$

$$T_2 = 2\eta_2 D \tag{3b}$$

$$\mathrm{T}_1 = \frac{G}{\xi}(3\Lambda^2 S - \mathrm{I}) \tag{3c}$$

$$\lambda\left[\left(1-\frac{\xi}{2}\right)\overset{\nabla}{S} + \frac{\xi}{2}\overset{\nabla}{S}\right] + \lambda(1-\xi)[2D : S]S + \frac{1}{\Lambda^2}\left[S - \frac{\mathrm{I}}{3}\right] = 0 \tag{3d}$$

$$\lambda_0\frac{DA}{Dt} - \lambda_s(\nabla v : S)\Lambda + (\Lambda - 1)e^{\frac{2(\Lambda-1)}{q}} = 0 \tag{3e}$$

where q in *Eq. 3e* is the maximum stretching that a molecule can undergo. It represents a strain hardening behavior.

The simplified viscoelastic model represents extra stress as [45]:

$$\mathbf{T} = \begin{pmatrix} \psi\mu(\dot{\chi})\dot{\chi} & \eta(\dot{\gamma})\dot{\gamma} & \cdot \\ \eta(\dot{\gamma})\dot{\gamma} & \cdot & \cdot \\ \cdot & \cdot & \cdot \end{pmatrix} \tag{4}$$

where μ is the normal viscosity, η is a shear viscosity, and Ψ is a weighting coefficient representing the die swell. Ψ is an amplitude of the die swell and is determined by experiments and simulations [46]. The Bird–Carreau model was used for the normal and shear viscosity models in *Eq. 4*, as well as the generalized Newtonian flow simulation [3]. Parameters used in this study for the various rheological models are shown in Table 1.

Determination of Relaxation Time and Parameters. Three relaxation modes were used in the viscoelastic simulations. The determination of the relaxation times has been described [44]. The basis relaxation time was set to the reciprocal of the mean shear rate that was determined using the generalized Newtonian analysis, as described in the previous article. The minimum and maximum relaxation times ($\lambda_{\min}$ and $\lambda_{\max}$) were calculated using basis relaxation time (λ_B) as follows: $\lambda_{\min} = \lambda_B/3$ and $\lambda_{\max} = \lambda_B \cdot 3$. The parameters in each viscoelastic model were determined using curve fitting in Polyflow with the material data shown in Fig. 1.

RESULTS AND DISCUSSION

Pressure and Velocity Distributions

The pressure distribution in the reservoir and capillary die is shown in Fig. 3a. The pressure in the reservoir is very low

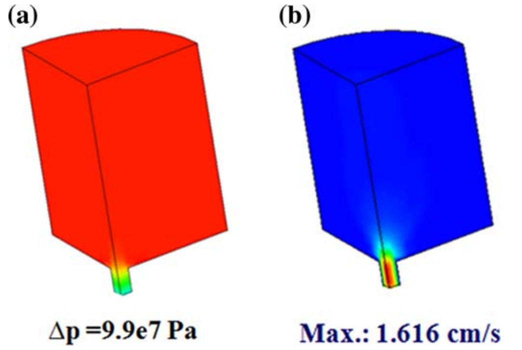

FIG. 3. Predicted pressure and velocity distributions. (a) Pressure distribution for the Giesekus model. (b) Velocity distribution for the POMPOM model. [Color figure can be viewed in the online issue, which is available at wileyonlinelibrary.com.]

and as the material approaches the capillary die, the pressure increases significantly. All rheological models exhibited similar tendencies in pressure distribution. However, the amount of the driving pressure ($\Delta p_{\rm d}$) between the inlet and outlet was different. The velocity distributions in the reservoir and the capillary die are shown in Fig. 3b for the POMPOM model. The velocity at the reservoir was very low and it began to increase near the capillary die, whereas that in the center region of the capillary die exhibited the highest value. Table 2 summarizes predicted driving pressures and maximum velocities in the capillary die for the five models investigated. Comparing the maximum velocities for each model, the full viscoelastic models (PTT, Giesekus, and POMPOM models) exhibited a higher maximum velocity than the generalized Newtonian and simplified viscoelastic models. However, the velocity distributions were similar for all models investigated in this research.

Velocity Profiles

The velocity profiles at the cross section of the capillary die length are shown in Fig. 4. The velocities in the center region are clearly higher than for the other regions, and the velocities in the center region of the PTT and Giesekus models were significantly higher than for those of the other models. The velocity profiles in a center region for the POMPOM and generalized Newtonian models were flat, whereas those near the walls decreased steeply. The velocity profiles of the PTT and Giesekus models were comparative to those of the POMPOM and generalized Newtonian models. The different velocity profiles exhibited different velocity gradients and shear rates. Consequently, the different rheological models exhibited different shear rates. The different shear rates also exhibited different rheological and thermal behaviors because those depend on the shear rate. The velocity profiles of the power law fluid according to the power law index in a circular die are dominated as described by [1]:

TABLE 2. Predicted driving pressure and maximum velocity in the capillary die for various rheological models.

Model	Predicted Driving Pressure (ΔP_d)[a][Pa]	Max. Velocity in The Capillary Die [cm/sec]
PTT	8.28e7	1.614
Giesekus	9.9e7	1.718
POMPOM	8.66e6	1.616
Simplified Viscoelastic	3.32e6	1.293
Generalized Newtonian	5.70e6	1.295

[a]Driving pressure (ΔP_d): pressure at reservoir entrance – pressure at die exit

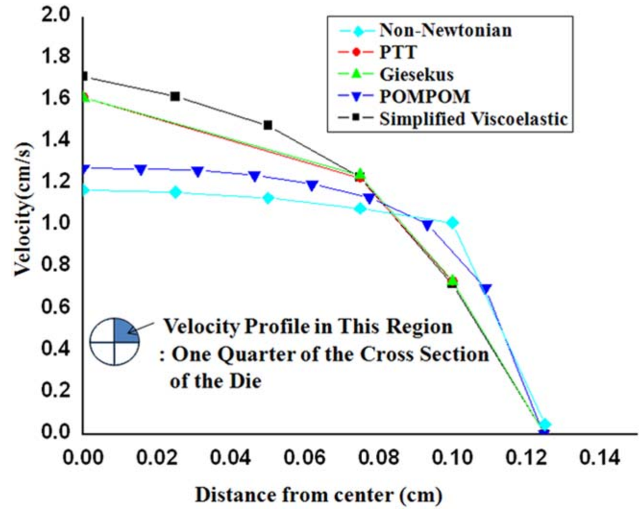

FIG. 4. Computation results of the velocity profiles at the capillary die cross section. [Color figure can be viewed in the online issue, which is available at wileyonlinelibrary.com.]

$$v_z=\left[\frac{1}{2K}\frac{\partial p}{\partial z}\right]^{\frac{1}{n}}\left(\frac{n}{1+n}\right)R^{\frac{1}{n}+1}\left[1-\left(\frac{r}{R}\right)^{\frac{1}{n}+1}\right] \tag{5}$$

When the power law index is large, the velocity profile becomes sharp at the center. The sharpest velocity profile is for the Newtonian model, at $n=1$. As the nonlinearity increases, the velocity profile in the center region becomes flat. The velocity profiles of the POMPOM model resemble the power law model with a high power law index.

Pressure Profiles

Figure 5 presents the pressure profiles along the flow direction from the inlet of the reservoir to the exit of the capillary die according to the *L*/*D*. High pressures were required in the reservoir for longer dies in order to maintain the same flow rate. The PTT and Giesekus models predicted higher pressure in the reservoir compared with the POMPOM, simplified viscoelastic, and generalized Newtonian models. The pressure decreased as the flow approached the capillary die entrance and fell at the die entrance. The pressure drop at the capillary die entrance is denoted by ΔP and depicted in Fig. 5. The rheological models that predicted a high pressure in the reservoir exhibited high pressure drops. The POMPOM, simplified viscoelastic, and generalized Newtonian models predicted small pressure drops compared with the other models investigated. The pressure profiles for the various models are compared in Fig. 6. The PTT and Giesekus models exhibited higher pressure profiles than the other models investigated. Furthermore, the PTT and

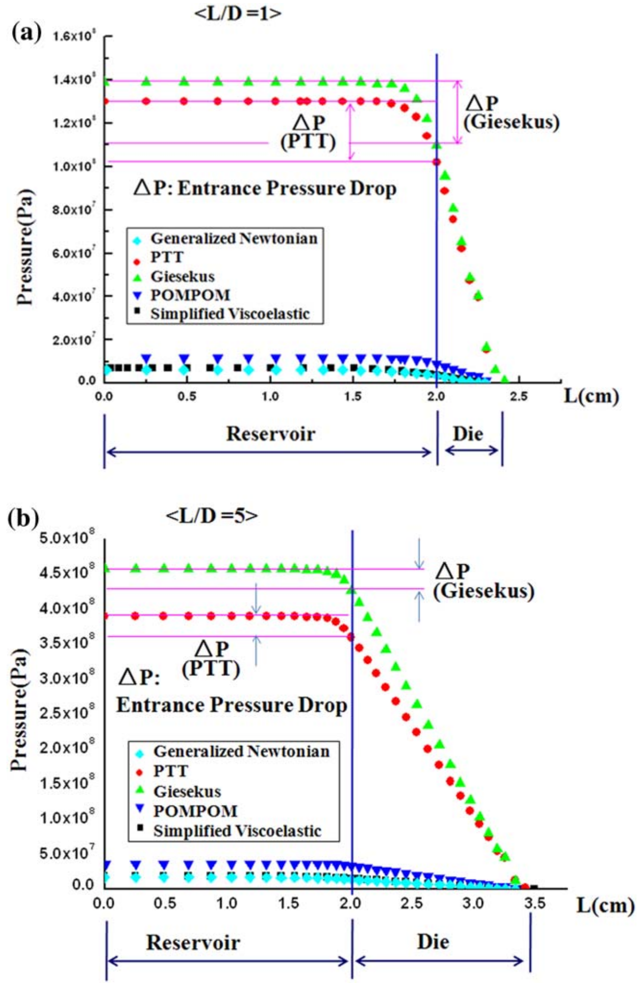

FIG. 5. Pressure profiles from the reservoir to the capillary die in the flow direction and die entrance pressure drops (Δp) for the various rheological models. (a) $L/D = 1$ and (b) $L/D = 5$. [Color figure can be viewed in the online issue, which is available at wileyonlinelibrary.com.]

Giesekus models predicted more than one order of higher pressures in the reservoir compared with the other models investigated. Although the pressure levels according to the L/D differed, the profiles were similar to each other.

Pressure Drops and Pressure Drop Ratios at the Die Entrance

Pressure drops at capillary die entrances are well-known phenomena [2]. The pressure drop and pressure drop ratio at the capillary die entrance for various rheological models and various L/D values are shown in Figs. 7 and 8. Figures 5 and 6 represent the pressure profiles from the reservoir inlet to the capillary die outlet for different models. The definition of a pressure drop (ΔP) at the capillary die entrance is shown in Fig. 5. The pressure drops may be divided into two groups based on the amount of the drops: those predicted by the PTT and Giesekus models versus those predicted by the POMPOM, simplified viscoelastic, and generalized Newtonian models. The PTT and Giesekus models exhibited high pressure drop at the capillary die entrance compared with the other models (Fig. 7). The pressure drop increased as the capillary die length increased from $L/D = 1$ to $L/D = 5$ (Fig. 7). The pressure drop ratio (%), which is the ratio of the entrance pressure drop to the reservoir pressure, is shown in Fig. 8. The pressure drop ratios are also divided into two groups according to the amount of pressure drop: the results from the simplified viscoelastic and generalized Newtonian models versus those from the PTT, Giesekus, and POMPOM models are shown in Fig. 8. The simplified viscoelastic and generalized Newtonian models exhibited higher pressure drop ratios compared with the other models. As the die length increases, the pressure drop increases as shown in Fig. 7; however, the pressure drop ratio decreases as the die length increases as shown in Fig. 8. The pressure drop ratios for $L/D = 1$ are 20–25% for the three viscoelastic models (PTT, Giesekus, and POMPOM models) and 44–46% for the simplified viscoelastic and generalized Newtonian models. However, the pressure drop ratios decreased to between 2 and 8% for $L/D = 15$. Figure 8 represents the pressure drop ratios for the different L/D values. As the die length increases, the pressure drop ratio decreases. The differences in the pressure drop ratios according to the rheological models decreased as the L/D increased.

Die Entrance Vortexes

A typical viscoelastic flow behavior is a vortex near sudden contraction regions; Fig. 9 represents the vortices of the flows. The full viscoelastic models (PTT, Giesekus, and POMPOM models) exhibited vortices at the corner of the reservoir, whereas the generalized Newtonian and simplified viscoelastic models did not exhibit vortices at all. Through this study it was understood that the full viscoelastic models could predict detailed viscoelastic flow behaviors. The vortex changes according to the L/D are shown in Fig. 10 for the PTT, Giesekus, and POMPOM models. The vortices decreased as the L/D of the capillary die increased; this indicates that the flows are more stable for longer dies.

Die Swells

Die swell in the extrusion of rubber compounds is a very important flow behavior in die design. Consequently, the prediction and measurement of the die swell is essential. Figure 11 represents the die swells according to flow rate for the different rheological models and the experimental results for $L/D = 1$. The die swells increased as the flow rate increased. The die swell is a function of the shear rate; thus, it increases as the flow rate increases. The measured die swells were distributed between 1.25 and 1.32; the die swells predicted by the PTT and simplified viscoelastic models exhibited good agreement with the experiment. The die swell predicted by the POMPOM model was the smallest among the models investigated.

CONCLUSIONS

In this study, several viscoelastic models (i.e., PTT, Giesekus, POMPOM, and simplified viscoelastic) were applied to the extrusion process using a capillary die. These models were also compared with the generalized Newtonian (Bird–Carreau) model.

There were various velocity profiles in the capillary die for the simulation models. The PTT and Giesekus models

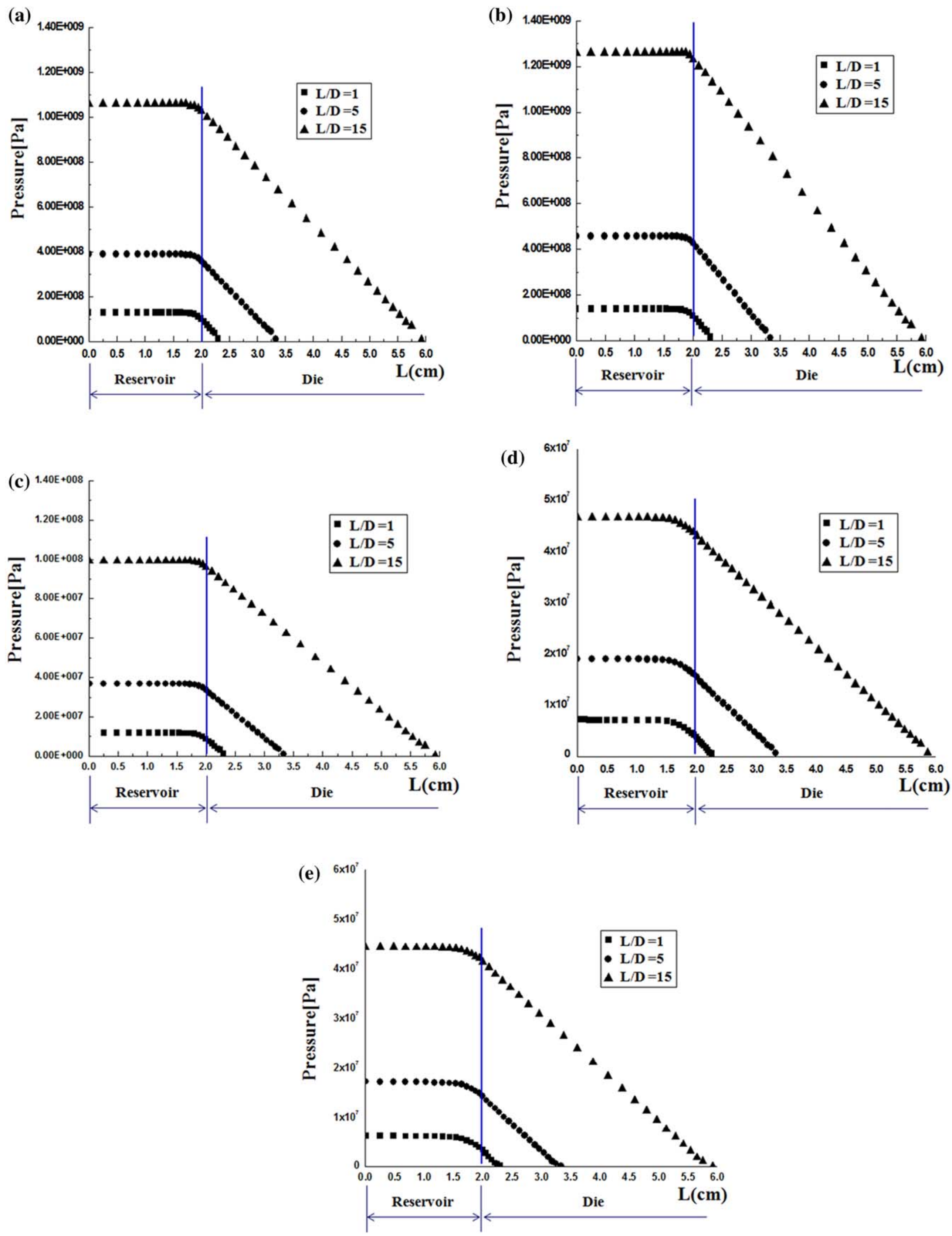

FIG. 6. Comparisons of the pressure profiles in the flow direction for various *L*/*D* values of the capillary die and rheological models. (a) PTT model, (b) Giesekus model, (c) POMPOM model, (d) simplified visco-elastic model, and (e) generalized Newtonian model. [Color figure can be viewed in the online issue, which is available at wileyonlinelibrary.com.]

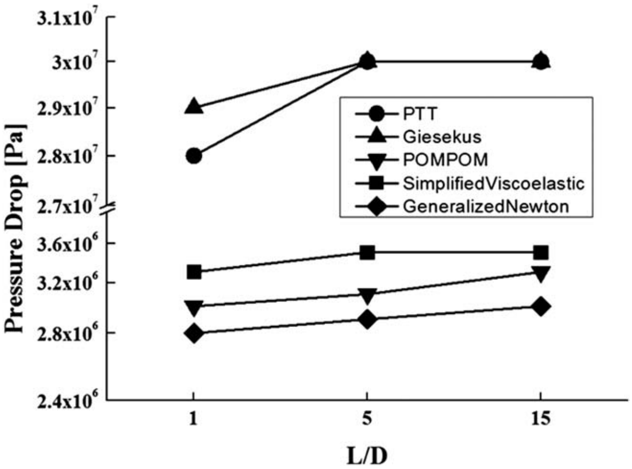

FIG. 7. Predicted pressure drops at the capillary die entrance according to the *L*/*D*.

exhibited sharp velocity profiles in the center region, whereas the velocity profiles from the generalized Newtonian, simplified viscoelastic, and POMPOM models were flat in the center region. The PTT and Giesekus models also exhibited high pressure in the reservoir compared with the other models. Highly viscous fluids need high pressures in order to maintain the flow; consequently, the PTT and Giesekus models predicted lower flow capability than the POMPOM, simplified viscoelastic, and generalized Newtonian models. Also the PTT and Giesekus models predicted higher pressure drops at the capillary die entrance than did the other models. However, the simplified viscoelastic and generalized Newtonian models predicted higher pressure drop ratios compared with the other models. The amount of pressure drop increased, but the pressure drop ratios decreased as the die length increased.

The full viscoelastic models (PTT, Giesekus, and POMPOM models) exhibited vortices in the corner of the capillary die entrance. However, the simplified viscoelastic and

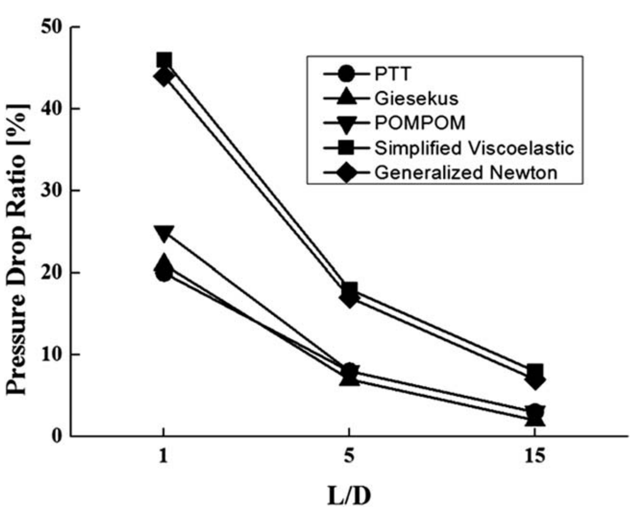

FIG. 8. Predicted pressure drop ratios at the capillary die entrance according to the *L*/*D* (pressure drop ratio = pressure drop at capillary die entrance/pressure in reservoir).

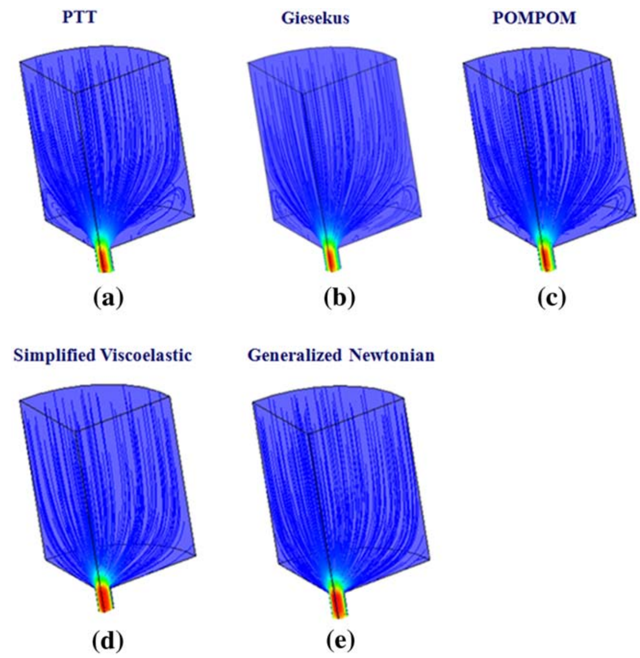

FIG. 9. Computational results of the vortexes at the corner of the capillary die entrance for the various rheological models. (a) PTT model, (b) Giesekus model, (c) POMPOM model, and (d) generalized Newtonian model. [Color figure can be viewed in the online issue, which is available at wileyonlinelibrary.com.]

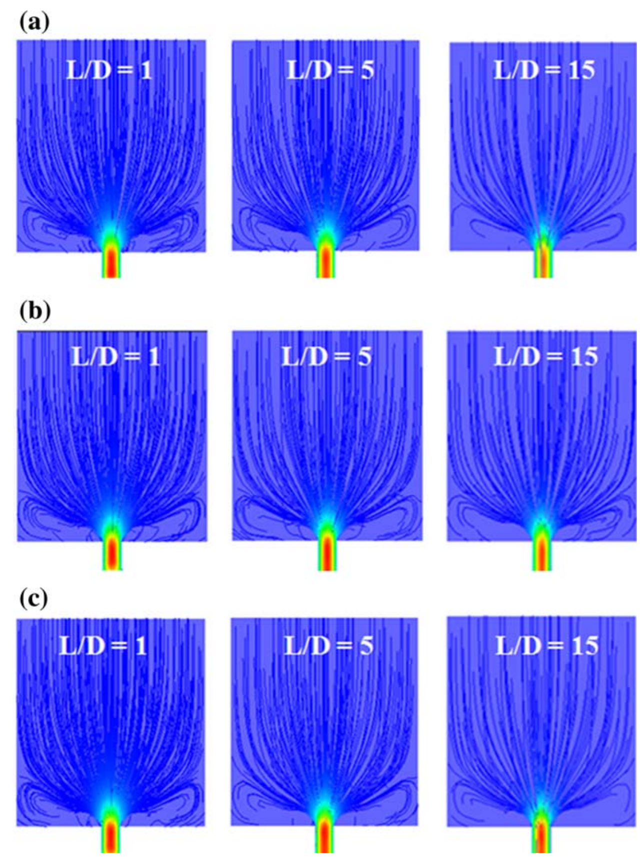

FIG. 10. Vortices at the corner of the capillary die entrance for various rheological models according to the *L*/*D*. (a) PTT model, (b) Giesekus model, and (c) POMPOM model. [Color figure can be viewed in the online issue, which is available at wileyonlinelibrary.com.]

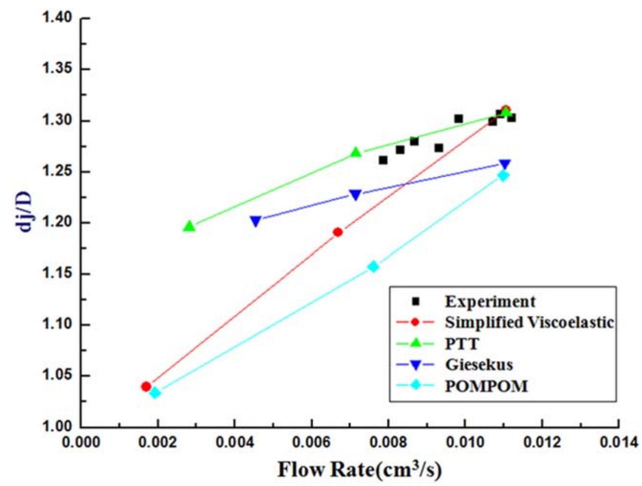

FIG. 11. Computation results of the die swells for the various rheological models compared with the experimental results. [Color figure can be viewed in the online issue, which is available at wileyonlinelibrary.com.]

generalized Newtonian models could not predict the vortices. The vortices decreased as the capillary die length increased; the pressure drop ratios at the capillary die entrance were more strongly related to the vortices in this region than to the pressure drops.

The die swells predicted by the tested models increased as the flow rate increased, and the measured die swells were between 1.25 and 1.32. Among the tested rheological models, the PTT and simplified viscoelastic models exhibited good agreement with the experiments. The simplified viscoelastic model had an advantage in computation time and simplicity in mathematical operation although it could not predict detailed viscoelastic flow behavior (the vortices).

REFERENCES

1. J.L. White, Principles of Polymer Engineering *Rheology*, Wiley, New York (1990).
2. C.D. Han, Rheology in Polymer *Processing*, Academic Press, New York (1976).
3. R.B. Bird, R.C. Armstrong, and O. Hassager, *Dynamics of Polymeric Liquids*: Vol. **1**, Wiley, New York (1987).
4. M.A. Hulsen, *Theor. Comput. Fluid Dyn.*, **5**, 33 (1993).
5. S.J. Park and S.J. Lee, *J. Non-Newtonian Fluid Mech.*, **87**, 197 (1999).
6. J.M. Kim, C. Chung, K.H. Ahn, and S.J. Lee, *Nihon Reoroji Gakkaishi*, **33**, 191 (2005).
7. R. Guenette and M. Fortin, *J. Non-Newtonian Fluid Mech.*, **60**, 27 (1995).
8. F.P.T. Baaijens, *J. Non-Newtonian Fluid Mech.*, **75**, 119 (1998).
9. H. Matallah, P. Townsend, and M.F. Webster, *J. Non-Newtonian Fluid Mech.*, **75**, 139 (1998).
10. M. Aboubacar and M.F. Webster, *J. Non-Newtonian Fluid Mech.*, **98**, 83 (2001).
11. F. Yurun and M.J. Crochet, *J. Non-Newtonian Fluid Mech.*, **57**, 283 (1995).
12. V. Ngamaramvaranggul and M.F. Webster, *Int. J. Numer. Methods Fluids*, **36**, 539 (2001).
13. J.-C. Huang and K.-S. Leong, *J. Appl. Polym. Sci.*, **84**, 1269 (2002).
14. H.W. Müllner, J. Eberhardsteiner, and K. Hofstetter, *Proc. Appl. Math. Mech.*, **6**, 575 (2006).
15. V. Ngamaramvaranggul and M.F. Webster, *Int. J. Numer. Methods Fluids*, **38**, 677 (2002).
16. Y. Kwon, *Polymer*, **25**, 536 (2001).
17. S.G. Hatzikiriakos and E. Mitsoulis, *Rheol. Acta*, **35**, 545 (1996).
18. E. Mitsoulis, S.G. Hatzikiriakos, K. Christodoulou, and D. Vlassopoulos, *Rheol. Acta*, **37**, 438 (1998).
19. E. Mitsoulis and S.G. Hatzikiriakos, *Rheol. Acta*, **42**, 309 (2003).
20. E. Mitsoulis, I.B. Kazatchkov, and S.G. Hatzikiriakos, *Rheol. Acta*, **44**, 418 (2005).
21. M. Ansari, A. Alabbas, E. Mitsoulis, and S.G. Hatzikiriakos, *Int. Polym. Proc.*, **25**, 287 (2010).
22. M. Ansari, E. Mitsoulis, and S.G. Hatzikiriakos, *Adv. Polym, Technol.*, **38**, 369 (2013).
23. S.H. Choi and M.-Y. Lyu, *Int. Polym. Proc.*, **24**, 326 (2009).
24. J.H. Kim, J.S. Hong, S.H. Choi, H.J. Kim, and M.-Y. Lyu, *Elastom. Compos.*, **46**, 54 (2011).
25. M.-Y. Lyu, D. Park, H. Kim, and J. Yoon, *Elastom. Compos.*, **41**, 223 (2006).
26. P.K. Agarwal, E.B. Bagley, and C.T. Hill, *Polym. Eng. Sci.*, **18**, 282 (1978).
27. M.A. Huneault, P.G. Lafleur, and P.J. Carreau, *Plast. Eng.*, **18**, 39 (1989).
28. N. Sombatsompop and S. Sergsiri, *Polym. Adv. Technol.*, **15**, 472 (2004).
29. J.-Z. Liang, *J. Appl. Polym. Sci.*, **104**, 70 (2007).
30. J.-C. Huang and Z. Tao, *J. Appl. Polym. Sci.*, **87**, 1587 (2003).
31. H.W. Müllner, J. Eberhardsteiner, and W. Fidi, *Polym. Test.*, **26**, 1041 (2007).
32. R.I. Tanner, *J. Non-Newtonian Fluid Mech.*, **129**, 85 (2005).
33. J.-Z. Liang, *Polym. Test.*, **20**, 29 (2000).
34. J. Vlachopoulos, *Rubber Chem. Technol.*, **51**, 133 (1978).
35. Y. Yang and L.J. Lee, *Polym. Eng. Sci.*, **27**, 1088 (1987).
36. N. Sombatsompop and R. Dangtangee, *J. Appl. Polym. Sci.*, **86**, 1762 (2002).
37. N. Sombatsompop and R. Dangtangee, *J. Appl. Polym. Sci.*, **82**, 2525 (2001).
38. W.A. Gifford, *Polym. Eng. Sci.*, **38**, 1167 (1998).
39. N. Tokita, *Rubber Chem. Technol.*, **54**, 439 (1981).
40. L. Gast and W. Ellingson, *Int. J. Numer. Methods Fluids*, **29**, 1 (1999).
41. S. Montes and J.L. White, *J. Non-Newtonian Fluid Mech.*, **49**, 277 (1993).
42. N. Phan-Thien and R.I. Tanner, *J. Non-Newtonian Fluid Mech.*, **2**, 353 (1977).
43. C.W. Macosko, *Rheology: Principles, Measurements, and Applications*, Wiley, New York (1994).
44. W.M.H. Verbeeten, G.W.M. Peters, and F.P.T. Baaijens, *J. Rheol.*, **45**, 823 (2001).
45. J. Mallet, H. Metwally, A. Dozolme, and B. Debbaut, *American Chemical Society: Rubber Division Technical Meeting & Business Summit*, 141 (2007).
46. J.H. Kim, H. Kim, M.-Y. Lyu, S.H. Choi, and H.J. Kim, *ANTEC*, **2**, 984 (2012).